Eur. Phys. J. Spec. Top. (2021) 230:1355–1370
https://doi.org/10.1140/epjs/s11734-021-00039-7

THE EUROPEAN PHYSICAL JOURNAL SPECIAL TOPICS

Regular Article

Unsteady MHD flow of a Williamson nanofluid on a permeable stretching surface with radiation and chemical reaction effects

R. Meenakumari[1], P. Lakshminarayana[1,a], and K. Vajravelu[2]

[1] Department of Mathematics, SAS, VIT, Vellore 632014, India
[2] Department of Mathematics, University of Central Florida, Orlando, FL 32816-1364, USA

Received 27 October 2020 / Accepted 31 January 2021 / Published online 12 April 2021

Abstract In the present work, we emphasize the impacts of an inclined magnetic field, viscous dissipation and radiation on the unsteady flow of a Williamson nanofluid over a vertical stretching porous surface with the presence of non-uniform heat source/sink and chemical reaction. In this study, we considered different kinds of nanoparticles such as silver, copper, aluminium oxide (Al_2O_3), titanium oxide (TiO_2), and magnesium oxide (MgO). The basic equations of this investigation are transmuted into a system of nonlinear and coupled ODEs using suitable similarity variables and elucidated numerically by R.-K. Fehlberg-based shooting technique. Influences of the pertinent parameters on the velocity, the temperature and the concentration distributions are deliberated with the assistance of graphs and tables. This study depicts that Al_2O_3 nanofluid has greater velocity since it has less dense nanoparticles compared to other nanoparticles. However, Cu-nanofluid has greater heat transfer due to greater thermal conductivity. Further, we identified that the thermal boundary layer thickness can be increased with the help of the viscous dissipation parameter. The inclination angle of the magnetic field strengthens the magnetic field on the fluid flow

List of symbols

u, v	Velocities in x- and y-direction (m/s)
g	Acceleration due to gravity (ms^{-2})
ϕ	Nanoparticle solid volume fraction (nm)
ρ_f, ρ_s	Densities of the base fluid and solid nanoparticles (kg/m^3)
ν_f	Kinematic viscosity of the fluid (m^2/s)
μ_f	Dynamic viscosity of the base fluid (kg/ms)
ρ_{nf}	Density of the nanofluid (kg/m^3K)
μ_{nf}	Effective dynamic viscosity of nanofluid (kg/ms)
σ_{nf}	Electrical conductivity of the nanofluid (S/m)
α_{nf}	Thermal diffusivity of the nanofluid
β_{nf}	Thermal expansion of the nanofluid
k_{nf}	Thermal conductivity of the nanofluid (W/m K)
C_p	Specific heat capacity (J/kg K)
σ_f, σ_s	Electrical conductivities of the base fluid and solid fraction
$(\rho\beta)_f (\rho\beta)_s$	Thermal expansion coefficient of the base fluid and solid fraction
$(\rho C_p)_f, (\rho C_p)_s$	Heat capacities of the base fluid and solid fraction
k_f, k_s	Thermal conductivities of the base fluid and Solid fraction
k	Thermal conductivity
η	Similarity variable
f	Dimensionless velocity
θ	Dimensionless temperature
Φ	Dimensionless concentration
$A = \frac{\alpha}{a}$	Unsteadiness parameter
$We = \sqrt{2}\Gamma\sqrt{\frac{a^3}{\nu_f(1-\alpha t)^3}}$	Fluid parameter
H	Magnetic parameter
λ	Buoyancy or convection parameter
γ	Angle of inclination
K	Permeability parameter
$A*$	Space-dependent heat source/sink
$B*$	Temperature-dependent heat source/sink

[a] e-mail: laxminarayana.pallava@gmail.com (corresponding author)

R	Radiation parameter
$\mathrm{Ec} = \frac{U_w^2}{(T_w - T_\infty)}$	Eckert number (viscous dissipation parameter)
$\mathrm{Pr} = \frac{(\rho C_p)\nu_f}{k_f}$	Prandtl number
$\mathrm{Sc} = \frac{\nu_f}{D_B}$	Schmidt number
$\mathrm{Re}_x = \frac{u_w x}{\nu_f}$	Local Reynolds number
K_r	Chemical reaction parameter
C_{fx}	Skin friction coefficient
Nu_x	Nusselt number
Sh_x	Sherwood number

1 Introduction

Nanotechnology is an emerging science. A nanoparticle is a microscopic particle that is incredibly small with small diameters (1–100 nm) such as metals, oxide and semiconductor nanoparticles. Generally, nanoparticles have excellent conductivity and catalytic properties. Different kinds of nanoparticles of various sizes and shapes suspended in different base fluids can change the heat transfer characteristics of the base fluid. Nanoparticles are widely used in biotechnology and pharmacology etc. Nanofluid is a fluid containing nano-sized particles in the base fluid. The heat transfer properties of nanofluids are relying on thermal properties, shape and size of dispersed particles. Nanofluids act as a smart fluid, where the heat transfer can be reduced or enhanced. The nanofluids have high thermal conductivity as compared to the base fluids like water, oil or ethylene glycol mixtures. Choi [1] was the first person who developed the terminology of nanofluids. He invented nanoparticles suspended in the base fluid that have greater thermal conductivity and higher heat conduction than pure fluids. Eastman [2] tested the thermal conductivity of nanofluids with different nanoparticles in two different base fluids. In the experimental results, he found that the nanofluids are performed 60% greater thermal conductivity as compared to that of the corresponding base fluid with a small amount of volume fraction (usually less than 5%).

Hang Xu et al. [3] scrutinized the heat transport characteristics of unsteady liquid over a horizontal enlarging surface by taking three different nanoparticles. He perceived that the nanoparticle dispersion improves the rate of heat transfer by increasing nanoparticle volume fraction and the rate of heat transfer is lesser in the case of Cu–water nanofluid than Al_2O_3-water nanofluid. Vajravelu et al. [4] studied the impacts of variable thermal conductivity and radiation on an unsteady viscous fluid flow and heat transport characteristics at a stretching pane. In this investigation, they analysed the effects of suction and injection on the velocity and temperature distribution for both unsteady and steady flows and concluded that the velocity and the temperature fall with growth in the unsteady parameter. Yanhai Lin et al. [5] examined the viscous dissipation and variable thermal conductivity effects on unsteady finite pseudo-plastic nanofluid at a stretching surface. They detected that the temperature declines for large values of Eckert number. A comparative study of non-Newtonian nanofluids was presented by Sandeep et al. [6]. They perceived that the heat and mass transfer rates are high in Oldroyd-B nanofluid than the Jeffery and Maxwell nanofluids.

Electrically conducting nanofluids have remarkable applications such as MHD pumps, conductors, generators, transformers, crystal growth, cooling of a nuclear reactor, biological transportation and drug delivery. Many researchers investigated the MHD nanofluid flows and heat transfer characteristics [7–10]. In recent years, researchers paid great attention to study non-Newtonian fluids because of its demanding industrial and engineering applications. Some examples of non-Newtonian fluids are emulsions, paints, many biological fluids, lubricants, honey, ketchup, etc. The common characteristics of these products are experiences in day-to-day life that fluids are not obeying the Newton's law of viscosity. According to the inherent thermophysical properties of the compound fluids, several fluid models have been proposed. These fluids are mainly classified into visco-elastic and inelastic. Some recent investigations of non-Newtonian fluids are given in the reference section [34–40]. Williamson fluid is a non-Newtonian fluid that yields shear thinning while increasing shear stress. Nadeem and Hussain [11–13] analysed the boundary layer flow of Williamson fluid by most popular analytical technique Homotopy analysis method. They conclude that the Williamson fluid flow describes pseudoplastic fluid because the velocity profiles decrease for an increase in the fluid parameter. Ramzan et al. [14] discussed the convective Williamson nanofluid flow with the impacts of radiation and chemical reactions over a Riga plate. Boundary layer flows of Williamson fluid with different geometries are investigated by the authors [15–21].

Thermal radiation plays a major role in engineering and industries, for example, polymer treating, nuclear reactor glass fabrication, solar power technology and astronomical technology, etc. Sheikholeslami et al. [22] numerically studied the influence of radiation and magnetic field on a nanofluid flow between two horizontal rotating parallel plates. Their results indicate that thermal boundary layer thickness declines with the growth in radiation parameter. The radiation effect on boundary layer flow with the convective boundary condition was investigated by Ishak et al. [23]. They noticed that the radiation and convective boundary conditions moderate the rate of heat transfer at the surfaces. Mahanthesh et al. [24] discussed the MHD mixed convective flow of chemically reacting nanofluid. They found that the addition of nanoparticle in the base fluid has the capability to improve the heat transfer performance. Vinodkumar and Lakshminarayana [46] examined the effects of radiation and chemical reaction on a conducting Maxwell fluid flow over a stretching surface.

Elgazery [25] studied the effect of magnetic field on a convective nanofluid flow over a permeable verti-

cal stretched surface. He concluded that the thermal boundary layer thickness is high in the case of TiO_2 nanofluid. Hayat et al. [26] investigated the heat transfer analysis of Ag–water and Cu–water nanofluids over an inclined cylinder in the presence of thermal radiation. Vajravelu [27] analysed the heat transport characteristics of Ag–water and Cu–water nanofluid over a stretching surface. Rohini et al. [28] discussed the effect of wall mass suction, unsteadiness and solid volume fraction in a water-based nanofluid containing different nanoparticles over a shrinking sheet. The authors [29–31] explained the effect of viscous dissipation on the boundary layer flow of different nanofluids. Sucharitha et al. [32] and Raju et al. [33] discussed the influence of aligned magnetic field on nanofluids. They concluded that the aligned magnetic field supports the magnetic field parameter and it can condense the flow.

In view of the aforementioned observations, we investigate the heat and mass transfer characteristics of base fluid and nanofluids (Cu-nanofluid and Al_2O_3-nanofluid) over an enlarging surface by considering MHD Williamson fluid with the existence of viscous dissipation, inclined magnetic field, radiation, non-uniform heat source/sink. The effect of influential parameters on velocity, temperature and concentration distributions are analysed with the graphical representation. The effects of physical parameters on the coefficient of skin friction, Nusselt number and Sherwood number are tabulated and explained. The present study is very useful in medicine and technology. Copper nanoparticle suspension in viscous fluids are taken for treatment of various cancers and pancreatic tumours. Alumina oxide nanoparticle suspension in viscous fluids is considered in cosmetic industries and food technology etc.

2 Formulation

We consider a two-dimensional unsteady MHD convective boundary layer flow of a Williamson nanofluid on a porous stretching sheet. The Williamson nanofluid contains different types of nanoparticles such as Ag, Cu, Al_2O_3, TiO_2 and MgO. The effects of MHD with an inclined magnetic field, convective heat and mass transfer, viscous dissipation, thermal radiation and heat generation/absorption are considered for the investigation. An aligned magnetic field B_o is applied to the stretched surface with an angle γ. The inclination angles are 0, 90° and $0 < \gamma < 90°$ represents the horizontal, vertical and inclined magnetic field models (see Fig.1).

The Constitute equation of the Williamson model is given as (see Nadeem [11])

$$S = pI + \tau$$
$$\tau = \left[\mu_\infty + \frac{\mu_0 - \mu_\infty}{1 - \Gamma\gamma}\right] A_1.$$

Here S is the extra tensor, μ_0 and μ_∞ are the limiting viscosities at zero and at infinite shear rate, $C > 0$ is

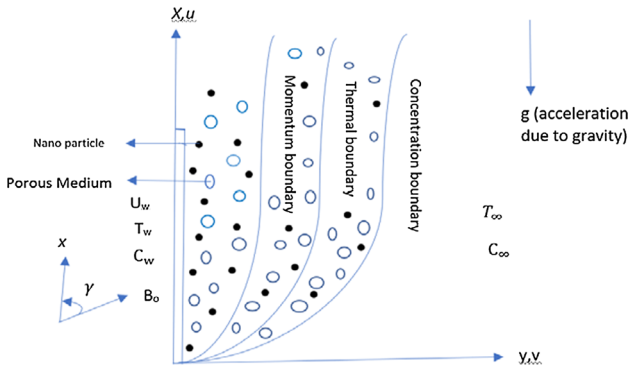

Fig. 1 Physical model

the time constant A_1 is the Rivlin-Ericksen tensor and defined as

$$A_1 = (\text{gradV}) + (\text{gradV})^{\text{T}}.$$

Here we have considered the case for which $\mu_\infty = 0$ and $\Gamma\gamma < 1$. Thus, the extra tensor takes the form

$$\tau = \left[\frac{\mu_0}{1 - \Gamma\gamma}\right] A_1.$$

The governing equations of the present study are [12, 47, 48]:

$$\frac{\partial u}{\partial x} + \frac{\partial v}{\partial y} = 0 \tag{1}$$

$$\frac{\partial u}{\partial t} + u\frac{\partial u}{\partial x} + v\frac{\partial u}{\partial y} = \frac{\mu_{\text{nf}}}{\rho_{\text{nf}}}\left(\frac{\partial^2 u}{\partial y^2} + \sqrt{2}\Gamma\frac{\partial u}{\partial y}\frac{\partial^2 u}{\partial y^2}\right) - \frac{\sigma_{\text{nf}}}{\rho_{\text{nf}}}B_0^2 \text{Sin}^2\gamma u + g\frac{(\rho\beta)_{nf}}{\rho_{\text{nf}}}(T - T_\infty) - \frac{\mu_{\text{nf}}}{\rho_{\text{nf}}K_1}u \tag{2}$$

$$\frac{\partial T}{\partial t} + u\frac{\partial T}{\partial x} + v\frac{\partial T}{\partial y} = \frac{k_{\text{nf}}}{(\rho C_p)_{\text{nf}}}\frac{\partial^2 T}{\partial y^2} - \frac{q'''}{(\rho C_{\text{p}})_{\text{nf}}} + \frac{1}{(\rho C_{\text{p}})_{\text{nf}}}\frac{\partial q_{\text{r}}}{\partial y} + \frac{\mu_{\text{nf}}}{(\rho C_{\text{p}})_{\text{nf}}}\left(\frac{\partial u}{\partial y}\right)^2 \tag{3}$$

$$\frac{\partial C}{\partial t} + u\frac{\partial C}{\partial x} + v\frac{\partial C}{\partial y} = D\frac{\partial^2 C}{\partial y^2} - K_{\text{r}}(C - C_\infty). \tag{4}$$

Boundary conditions

$$\left.\begin{array}{ll} u = U_{\text{w}} = \frac{ax}{1-\alpha t}, v = V_{\text{w}} = -\left(\frac{a\nu_f}{1-\alpha t}\right)^{1/2} f_{\text{w}}, & \\ T = T_{\text{w}} = T_\infty + \frac{bx}{(1-\alpha t)^2}, & \\ C = C_{\text{w}} = C_\infty + \frac{\text{bx}}{(1-\alpha t)^2} & \text{at } y = 0 \\ u = 0, T = T_\infty, C = C_\infty & \text{as } y \to 0, \end{array}\right\} \tag{5}$$

where U_{w} is the stretching velocity, V_{w} is the suction/injection velocity and T_{w} is the surface temperature, b is a constant as explained in [25]. Here $f_{\text{w}} > 0/f_{\text{w}} < 0$ is the suction/injection parameter.

The expressions for the thermophysical properties of the nanofluids are [25]:

$$\mu_{\mathrm{nf}} = \frac{\mu_{\mathrm{f}}}{(1-\phi)^{2.5}} \tag{6}$$

$$\left.\begin{array}{l} \rho_{\mathrm{nf}} = (1-\phi)\,\rho_{\mathrm{f}} + \phi\rho_{\mathrm{S}}, \\ \left(\rho C_{\mathrm{p}}\right)_{\mathrm{nf}} = (1-\phi)\,(\rho C_{\mathrm{p}})_f + (\rho C_{\mathrm{p}})_{\mathrm{s}}, \\ (\rho\beta)_{\mathrm{nf}} = (1-\phi)\,(\rho\beta)_{\mathrm{f}} + (\rho\beta)_{\mathrm{s}}\,, \\ \alpha_{\mathrm{nf}} = \frac{k_{\mathrm{nf}}}{\left(\rho C_{\mathrm{p}}\right)_{\mathrm{nf}}}, \sigma_{\mathrm{nf}} = (1-\phi)\,\sigma_{\mathrm{f}} + \phi\sigma_{\mathrm{s}} \end{array}\right\} \tag{7}$$

$$\frac{k_{\mathrm{nf}}}{k_{\mathrm{f}}} = \frac{(k_{\mathrm{s}}+2k_{\mathrm{f}}) - 2\phi(k_{\mathrm{f}}-k_{\mathrm{s}})}{(k_{\mathrm{s}}+2k_{\mathrm{f}}) + \phi(k_{\mathrm{f}}-k_{\mathrm{s}})}. \tag{8}$$

This equation is used only for spherical nanoparticles and this model is pertinent to examine the heat transfer performance using nanofluids

The dimensionless variables and stream functions are defined as follows:

$$\eta = y\left(\frac{a}{\nu_{\mathrm{f}}\,(1-\alpha t)}\right)^{1/2}, \psi = \left(\frac{a\nu_{\mathrm{f}}}{1-\alpha t}\right)^{1/2} x f\,(\eta)\,,$$
$$\theta\,(\eta) = \frac{T-T_\infty}{T_{\mathrm{w}}-T_\infty}, \Phi\,(\eta) = \frac{C-C_\infty}{C_{\mathrm{w}}-C_\infty}$$
$$u = \frac{\partial\psi}{\partial y} \text{ and } v = -\frac{\partial\psi}{\partial x}. \tag{9}$$

The velocity components u and v are expressed as follows:

$$u = \frac{ax}{1-\alpha t} f^{'}\,(\eta)\,, v = -\left(\frac{a\nu_{\mathrm{f}}}{1-\alpha t}\right)^{1/2} f\,(\eta)\,, \tag{10}$$

here Eq. (10) is satisfying the continuity equation (1).

By Rosseland approximation, we obtain [33]

$$\frac{\partial q_{\mathrm{r}}}{\partial y} = -\frac{16\sigma T_\infty^3}{3k^*}\frac{\partial^2 T}{\partial y^2}. \tag{11}$$

The non-uniform heat source/sink $q^{'''}$ is defined as

$$q^{'''} = \frac{k_{\mathrm{nf}} u_{w(x)}}{x\nu_{\mathrm{nf}}}\left(A^*\,(T_{\mathrm{w}}-T_\infty) + B^*\,(T-T_\infty)\right). \tag{12}$$

The positive values of A^* and B^* correspond to the internal heat source and the negative values of A^* and B^* correspond to the internal heat sink.

Substituting Eqs. (6)–(12) into the basic equations (1)–(5), the transformed ordinary differential equations and boundary conditions are presented below:

$$f^{'''}\left(1+\mathrm{Wef}^{''}\right) - (1-\phi)^{2.5}$$
$$\left\{M_1\left(\frac{f^{''}\eta A}{2} + Af^{'} + f^{'2} - ff^{''}\right) - M_2\lambda\theta + H\sin^2\gamma f^{'}\right\}$$
$$-Kf^{'} = 0 \tag{13}$$
$$\left(1+\frac{4}{3}\left(\frac{\mathrm{Rd}}{M_4}\right)\right)\theta^{''} - \frac{\mathrm{PrM_3}}{M_4}\left(\frac{\theta^{'}A\eta}{2} + 2A\theta + f^{'}\theta - f\theta^{'}\right)$$
$$+(1-\phi)^{2.5}\,M_1(A^*f^{'} + B^*\theta) + \frac{\mathrm{EcPr}}{M4(1-\phi)^{2.5}}f^{''^2} = 0 \tag{14}$$

$$\Phi^{''} - \mathrm{Sc}\left(\frac{\Phi^{'}A\eta}{2} + 2A\Phi + f^{'}\Phi - f\Phi^{'} + K_r\Phi\right) = 0. \tag{15}$$

The transformed boundary conditions are

$$\left.\begin{array}{ll} f = f_w, f^{'} = 1, \theta = 1, \Phi = 1 & \text{as } \eta \to 0 \\ f^{'} = 0, \theta = 0, \Phi = 0 & \text{as } \eta \to \infty \end{array}\right\}. \tag{16}$$

In addition to that, the constants M_1, M_2, M_3 and M_4 are given by

$$M_1 = (1-\phi) + \frac{\rho_{\mathrm{s}}}{\rho_{\mathrm{f}}}\phi, M_2 = (1-\phi) + \frac{(\rho\beta)_{\mathrm{s}}}{(\rho\beta)_{\mathrm{f}}}\phi, M_3$$
$$= (1-\phi) + \frac{(\rho C_{\mathrm{p}})_{\mathrm{s}}}{(\rho C_{\mathrm{p}})_{\mathrm{f}}}\phi,$$
$$M_4 = \frac{k_{\mathrm{nf}}}{k_{\mathrm{f}}} = \frac{(k_{\mathrm{s}}+2k_{\mathrm{f}}) - 2\phi(k_{\mathrm{f}}-k_{\mathrm{s}})}{(k_{\mathrm{s}}+2k_{\mathrm{f}}) + \phi(k_{\mathrm{f}}-k_{\mathrm{s}})}.$$

The local skin friction C_{fx} , the local Nusselt number Nu_x and the local Sherwood number Sh_x are defined as:

$$C_{\mathrm{fx}} = \frac{\tau_{\mathrm{w}}}{\rho_{\mathrm{f}}u_{\mathrm{w}}^2}, \mathrm{Nu}_x = \frac{xq_{\mathrm{w}}}{k_{\mathrm{f}}(T_{\mathrm{w}}-T_\infty)}, \mathrm{Sh}_x$$
$$= \frac{xJ_{\mathrm{w}}}{D_{\mathrm{B}}(C_{\mathrm{w}}-C_\infty)}. \tag{17}$$

Here τ_{w} is the wall shear stress, q_{w} is the wall heat flux and J_{w} is the surface mass flux, which are given by

$$\tau_{\mathrm{w}} = \mu_{\mathrm{nf}}\left(\frac{\partial u}{\partial y} + \frac{\Gamma}{\sqrt{2}}\left(\frac{\partial u}{\partial y}\right)^2\right)_{y=0},$$
$$q_w = -k_{\mathrm{nf}}\left(\frac{\partial T}{\partial y}\right)_{y=0}, J_{\mathrm{w}} = D_{\mathrm{B}}\left(\frac{\partial C}{\partial y}\right)_{y=0}. \tag{18}$$

Using the dimensionless variable (9) and (10) in Eqs. (17) and (18), we obtain

$$(\mathrm{Re}_x)^{1/2}\,C_{\mathrm{fx}} = \frac{1}{(1-\phi)^{2.5}}\left(f^{''} + \frac{\mathrm{We}}{2}f^{''2}\right),$$
$$\mathrm{Nu}_x(\mathrm{Re})^{(-1/2)}$$
$$= \left(1+\frac{4\mathrm{Rd}}{3\mathrm{M4}}\right)\theta^{''}, \mathrm{Sh}_x\,(\mathrm{Re})^{(-1/2)} = \Phi^{'}. \tag{19}$$

3 Numerical procedure

The governing PDEs (2–4) and the boundary conditions (5) are transformed in to a set of coupled and non-linear ODEs (13)–(15) with the boundary conditions (16) using the similarity transformation. The system of equations (13–15) has been solved numerically

using the Runge–Kutta-based shooting technique. We assumed uncertain initial conditions for unknown variables. The transmuted first-order differential equations are integrated numerically as an initial value problem to a given terminal node .We check the accuracy of the guess values of initial condition, by comparing the calculated value of different variable at the terminal node. The solution will converge when the difference between computed and given values is less. Suppose the solution is not convergent then we will modify the initial guesses and this process will continue until we get the accurate solution.

4 Discussion of the results

The influence of pertinent parameters namely magnetic parameter, unsteadiness parameter, fluid parameter, porosity parameter, convection parameter, Eckert number, heat generation/absorption parameters, Schmidt number and chemical reaction parameters are discussed in detail with the help of graphs and constructing tables for different values of various physical parameters. We consider different kinds of nanoparticles, namely Ag, Cu, Al_2O_3, TiO_2, MgO and Williamson fluid is taken as a base fluid for the present investigation. For the numerical computational purposes, in the entire study, we consider the nanoparticle volume fraction $\phi = 0$ for pure (Williamson) fluid and $\phi = 0.2$ for Williamson nanofluid. Further, we kept the following fixed values in the whole study except the varied values in figures: We $= 0.2$, $A = 0.1$, $H = 2$, Pr $= 21$, $\lambda = 0.2$, $\gamma = \pi/3$, $K = 0.2$, Ec $= 0.2$, $A^* = 0.3$, $B^* = 0.3$, $R = 0.5$, Sc $= 0.6$, $K_r = 0.2$.

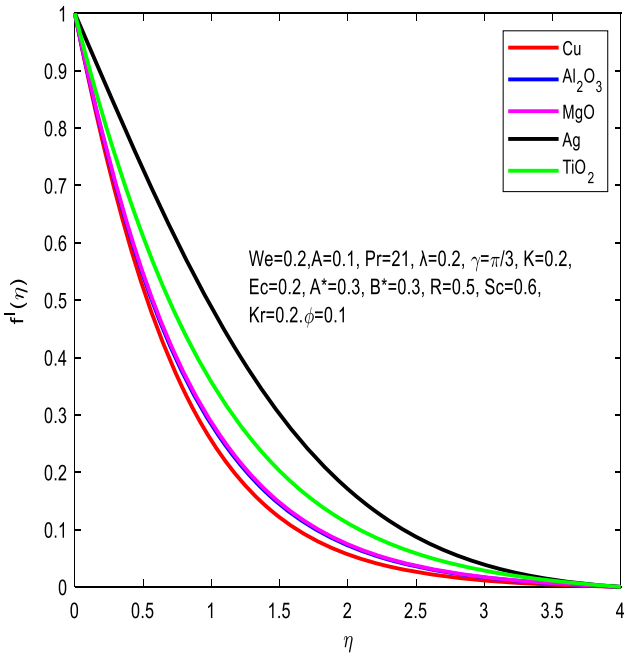

Fig. 2 Velocity distribution for different types of nanoparticles

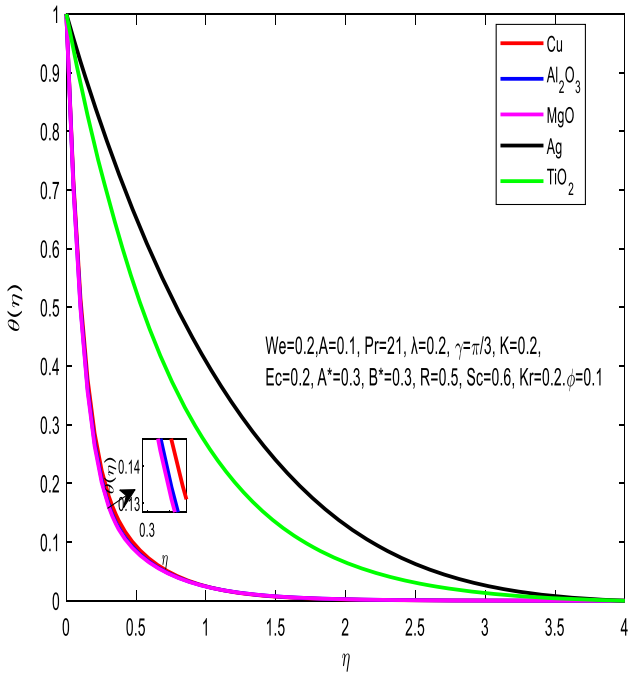

Fig. 3 Temperature distribution for different types of nanoparticles

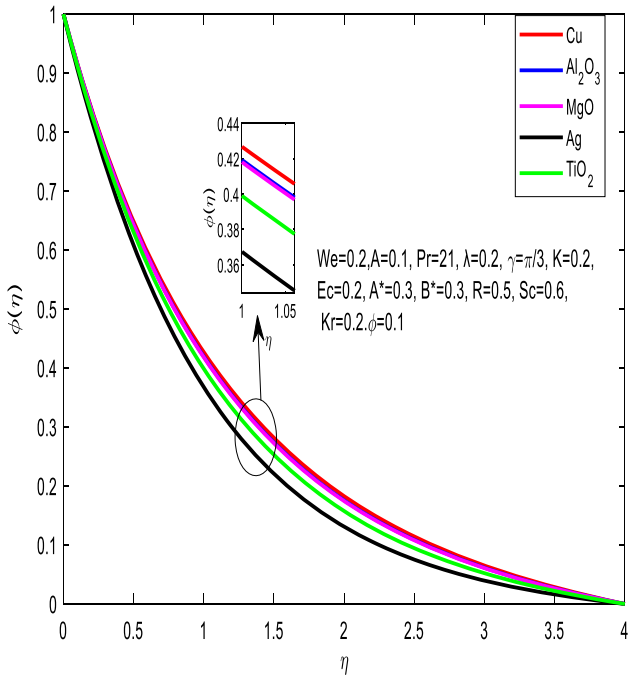

Fig. 4 Concentration distribution for different types of nanoparticles

Figures 2, 3 and 4 exhibit the variations in the flow for different nanoparticles mixed with the base fluid. We observed the variations in the velocity, temperature and concentration fields for different types of nanoparticles. Moreover, it is observed that the influence of Ag

nanofluid has maximum velocity compared with other nanofluids. Also, noticed that the inclusion of nanoparticles in the base fluid increases the density of the fluid which affects the thickness of the fluids. Figure 3 reveals that the silver based nanofluid attains maximum temperature and Mgo-based nanofluid has the minimum temperature. From this observation, we conclude that the thermal boundary layer is thicker for Ag-nanofluid. Figure 4 explains the impact of nanoparticles in concentration distribution. We perceived that the concentration boundary layer thickness is lesser for Ag-nanofluid when compared with the other nanofluids. The solutal boundary layer thickness of Al_2O_3-nanofluid is lesser than Cu-nanofluid. It is clear that the mass transfer is comparatively more in Cu-nanofluid than other nanofluids

Figures 5, 6 and 7 deliberate the variations in the velocity, temperature and concentration profiles of pure fluid and nanofluids for different values of the magnetic parameter, from these figures, it is noticed that the velocity profiles depletes for larger values of the magnetic parameter this is due to retarding nature of the drag force called Lorentz force that has the capability to controls the fluid motion and enhances the temperature. Also, found that the temperature of Cu and Al_2O_3 nanofluids is enhanced substantially as compared to that of pure fluid. Physically copper has more heat conduction than alumina which reveals in Fig. 6. Figure 7 shows the effect of the magnetic parameter on concentration. The concentration boundary layer thickness is increasing for raising values of the magnetic parameter. The concentration boundary layer is thicker for Al_2O_3 nanofluid

Figures 8, 9 and 10 exemplify the impact of A on the velocity, temperature and concentration for both pure

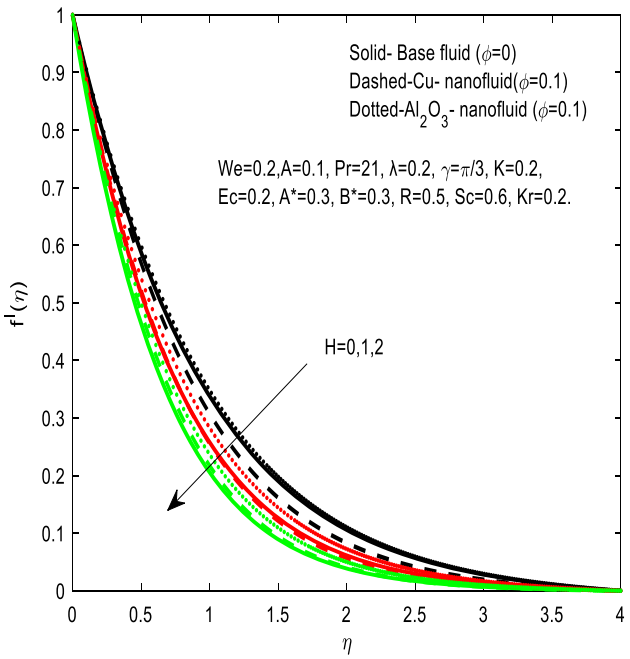

Fig. 5 Velocity profiles for H

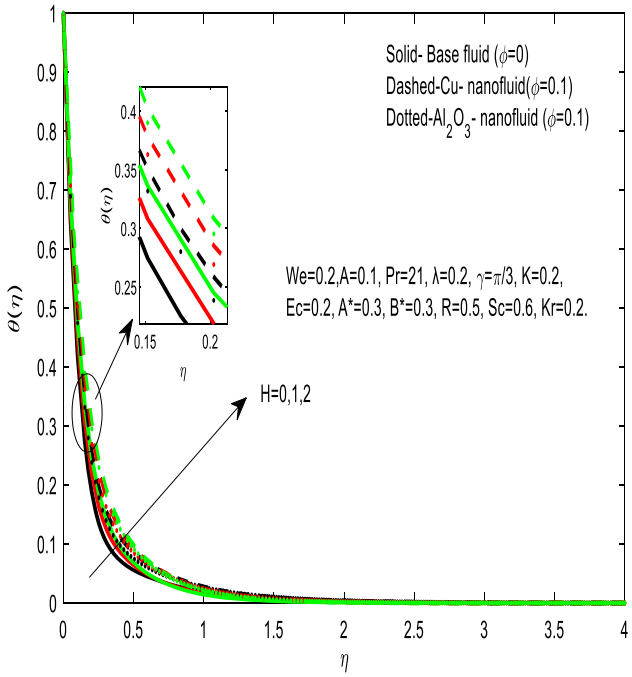

Fig. 6 Temperature profiles for H

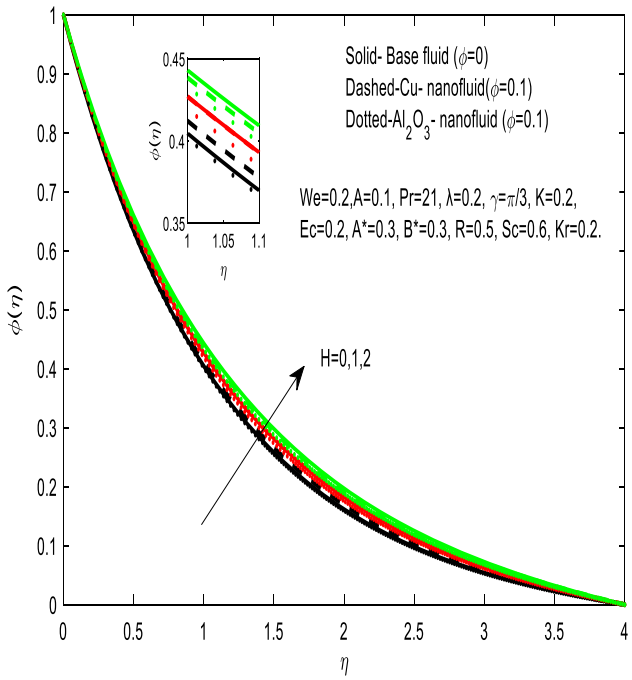

Fig. 7 Concentration profiles for H

fluid and nanofluids. From Fig.8, we noticed that the velocity distribution decelerates for increasing values of unsteadiness parameter and the associated momentum boundary layer thickness reduced. It is revealed that the momentum boundary layer of Al_2O_3-nanofluid is stronger than Cu-nanofluid for unsteadiness parameter. Figure 9 illustrates the temperature distribution for increasing values of the unsteadiness parame-

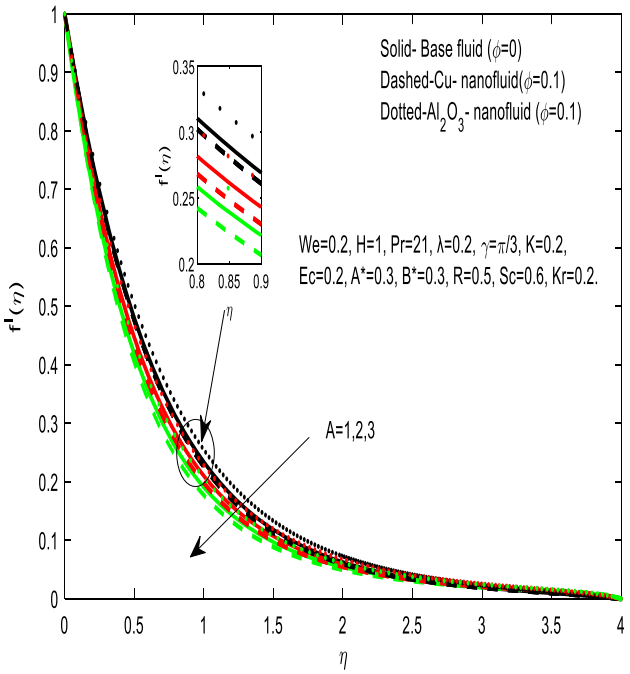

Fig. 8 Velocity profiles for A

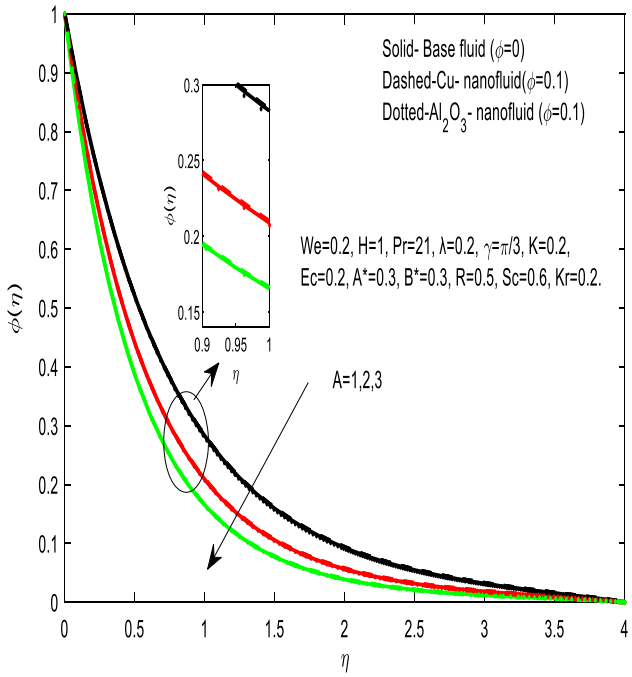

Fig. 10 Concentration profiles for A

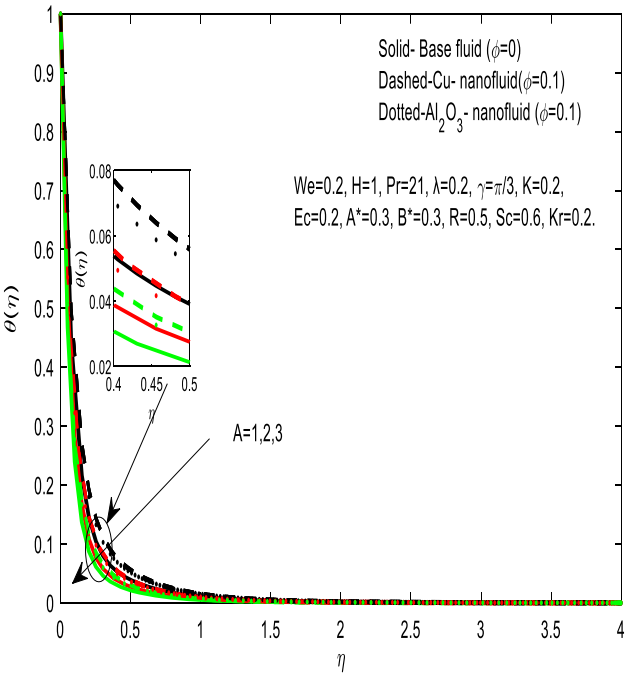

Fig. 9 Temperature profiles for A

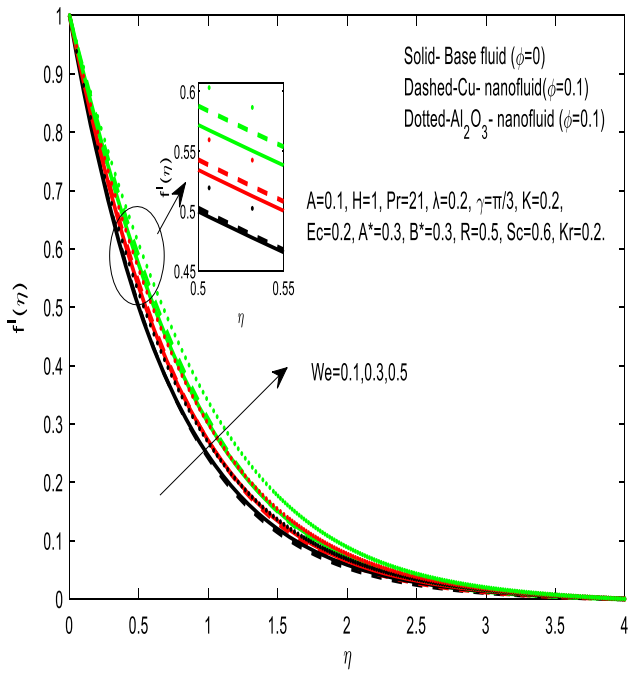

Fig. 11 Velocity profiles for We

ter. The temperature decelerates for higher values of the unsteadiness parameter and the temperature of nanofluids is stronger than the pure fluid. The effect of unsteadiness parameter on the concentration profile is displayed in Fig. 10. The concentration boundary layer is thinner for increasing values of the unsteadiness parameter. The concentration boundary layer of pure fluid is appreciably high as compared to the nanofluids.

Figures 11, 12 and 13 demonstrate the impact of the fluid parameter (We) on the present flow pattern. From Fig. 11, we noticed that the velocity enhances and the associated momentum boundary layer thickness increases for increasing values of the fluid parameter. The fluid parameter (We) measures the cause of viscosity to elasticity. We = 0 represents the Newtonian fluid and non-zero values of We corresponds to the purely viscoelastic fluid. The magnitude of the

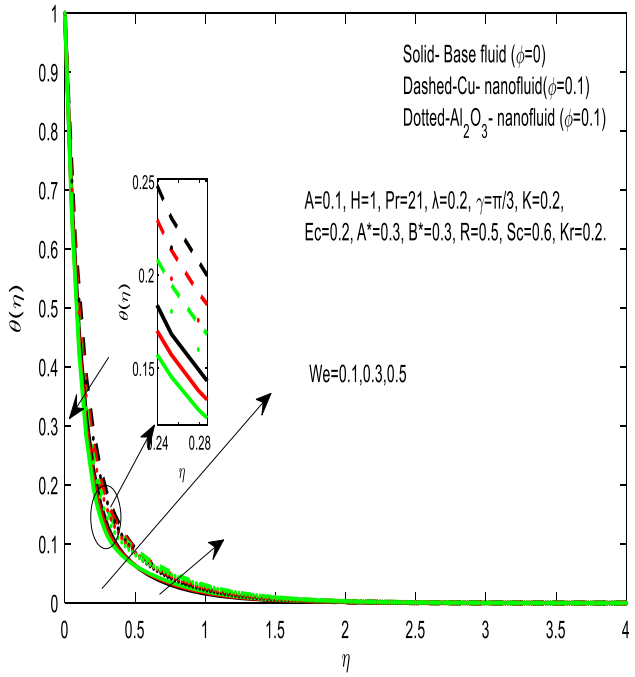

Fig. 12 Temperature profiles for We

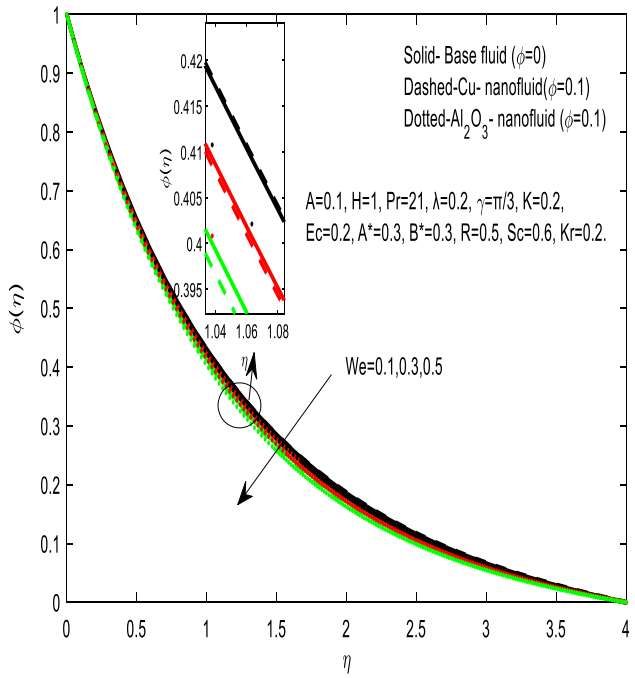

Fig. 13 Concentration profiles for We

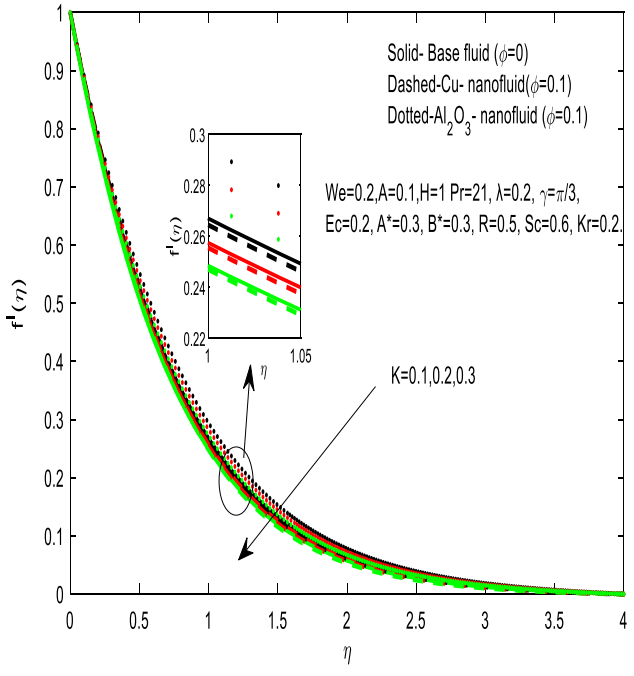

Fig. 14 Velocity profiles for different values of the porosity parameter K

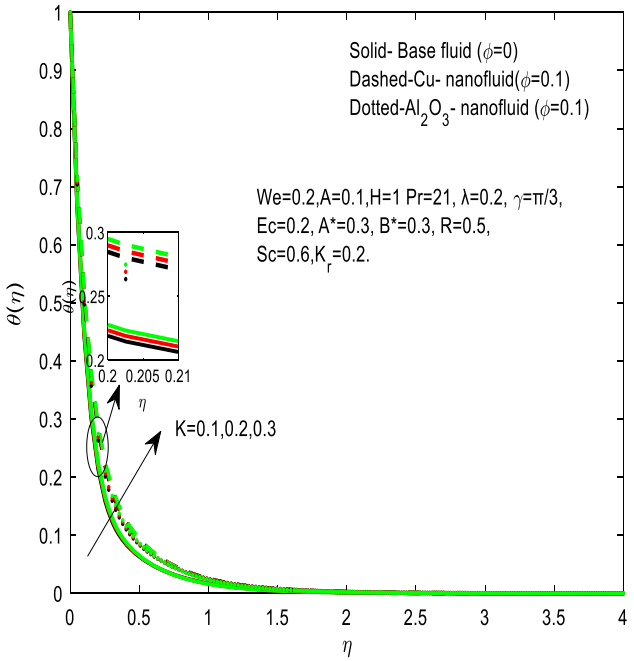

Fig. 15 Temperature profiles for different values of the porosity parameter K

velocity increases besides of the boundary layer for large values of We. Therefore, it decreases the cohesive forces between the fluid molecules. Thus, the momentum boundary layer is thicker for increasing values of the fluid parameter. The momentum boundary layer thickness of Al_2O_3 nanofluid is more than Cu-nanofluid.

Figure 12 portrays the impact of the We on the temperature field. We observed that the temperature depletes for different values of fluid parameter. Nanofluids are highly influenced the temperature distribution than that of pure fluid for larger values of We. The thermal boundary layer thickness of Cu-nano fluid is significantly high when compared to Al_2O_3-nanofluid.

Figure 13 presents the effect of We on the concentration field. The concentration boundary layer is

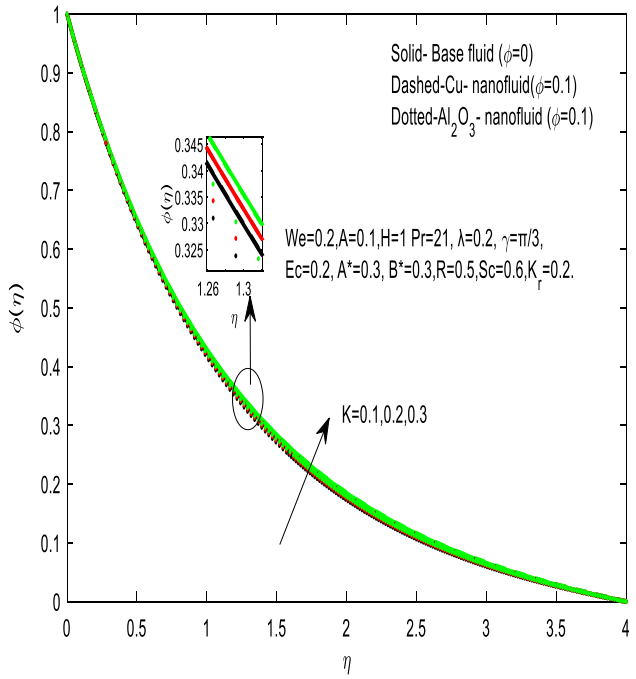

Fig. 16 Concentration profiles for different values of the porosity parameter K

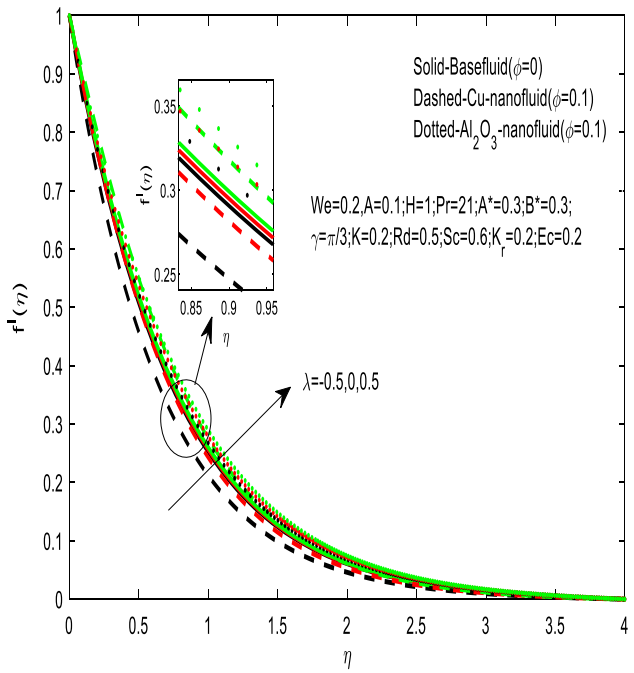

Fig. 17 Velocity profiles for λ

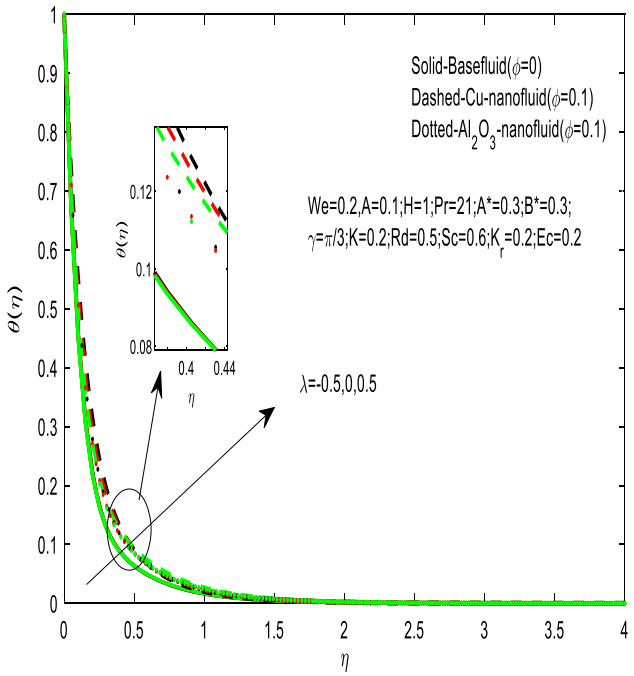

Fig. 18 Temperature profiles for λ

thinner for rising values of We. It is observed that the Cu nanofluid has more concentration than Al_2O_3-nanofluid. Figures 14, 15 and 16 explain the effect of K on the velocity, temperature and concentration distributions for both base fluid and nanofluids. In Fig. 14, we seen that the velocity declines for increasing values of K. It is noted that the presence of the porous medium slowdowns the fluid motion. Usually, the resistance of the flow increases with increasing porosity parameter. Due to this fact the velocity of the fluid falls down. It is seen that the momentum boundary layer is strongly influenced by Al_2O_3-nanofluid when compared with Cu-nanofluid. Figure 15 shows the temperature distribution for both pure fluid and nanofluids. The dominant values of K accelerate the temperature distribution and accompanying the thicker thermal boundary layer. The nanofluids are strongly influenced the temperature distribution than pure fluid for larger values of porosity parameter. The thermal boundary layer thickness of Cu-nano fluid is enhanced significantly when compared to Al_2O_3-nanofluid.

The effect of convection parameter on the fluid velocity, temperature and concentration fields for both pure fluid and nanofluids are displayed in Figs.17, 18 and 19. We observed an increment in the velocity field for large values of the λ. Due to the rise in the λ the temperature diminutions. Also, the temperature of nanofluids is stronger than the pure fluid. In particular, thermal boundary layer thickness of Cu-nanofluid is decreasing for higher values of convection parameter. Physically copper has more heat conduction than aluminium which comes out in present investigation. Figure 19 explores the effect of λ on the concentration field. The mass transfer of Cu-nanofluid is stronger than Al_2O_3-nanofluid.

Figures 20, 21 and 22 portray the effect of the suction/injection parameter (f_w) on the velocity, temperature and concentration fields for both pure and nanofluids. Figure 20 describes that the velocity distribution decelerates for ascending values of f_w. Suction/injection causes to fall in the momentum boundary layer thickness. Figures 21 and 22 show the behaviour of tem-

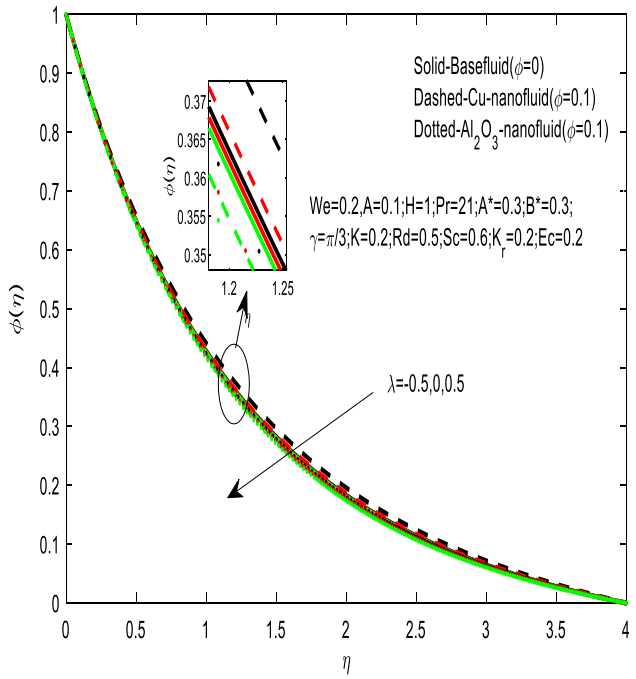

Fig. 19 Concentration profiles for λ

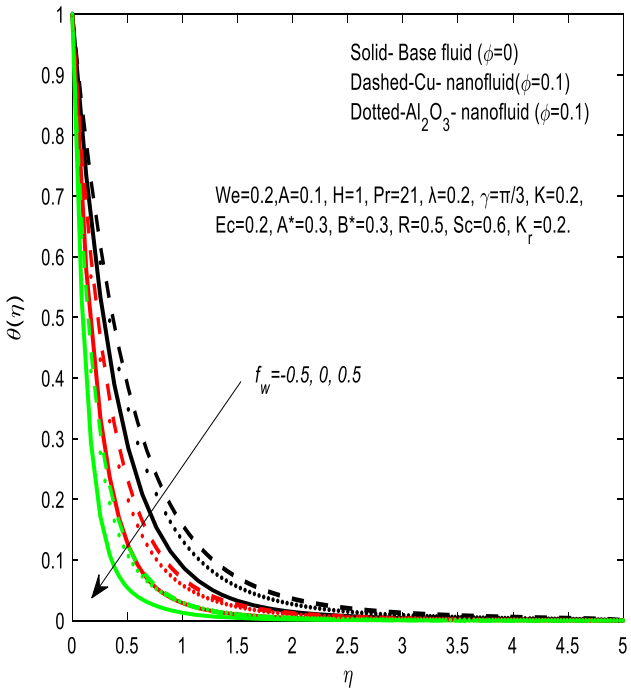

Fig. 21 Temperature profiles for f_{w}

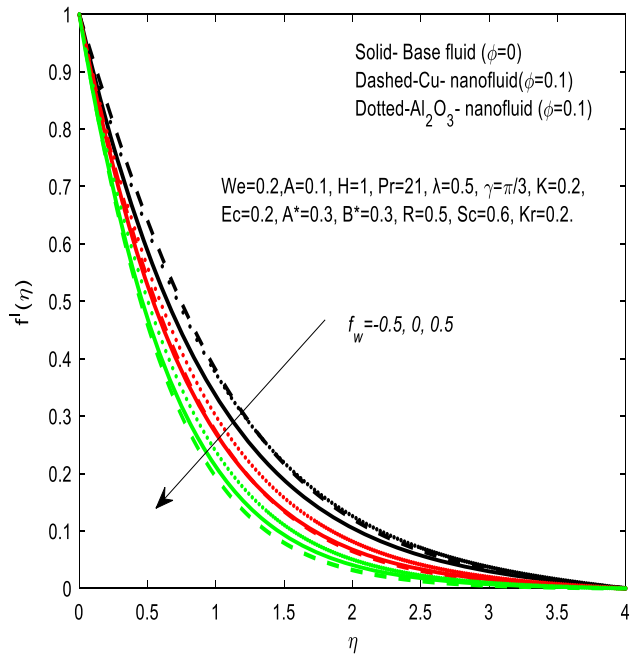

Fig. 20 Velocity profiles for f_{w}

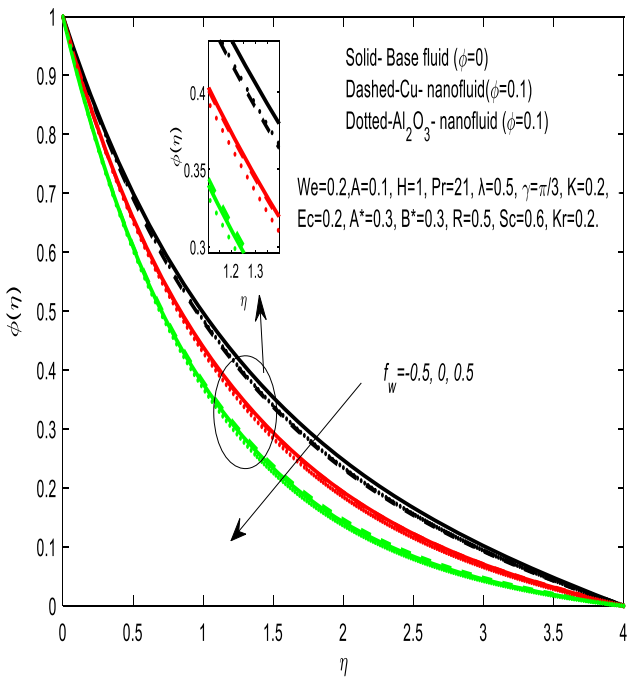

Fig. 22 Concentration profiles for f_{w}

perature concentration distributions for various values of f_{w}. We observed that the temperature and concentration fields are falling down for cumulative values of f_{w}. Further, we noticed that the thermal boundary layer thickness and solutal concentration field of Cu-nanofluid are comparatively higher than Al_2O_3-nanofluid.

Figures 23 and 24 depict that the velocity field decelerates for increasing values of the inclination angle of magnetic field. γ This has happened because an increment in γ fortify the magnetic field which enhances the Lorentz force. It reduces the momentum boundary layer thickness. Also, noted that Al_2O_3 nanofluid has a thin momentum boundary layer than Cu-nanofluid. We observed that the temperature profiles are high for rising values of γ The thermal boundary layer is strongly influenced by nanofluids when compared than the pure

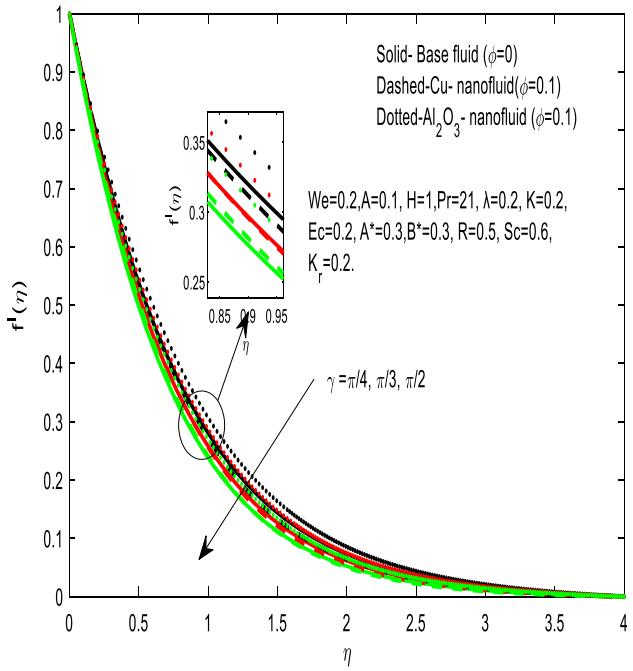

Fig. 23 Velocity profiles for γ

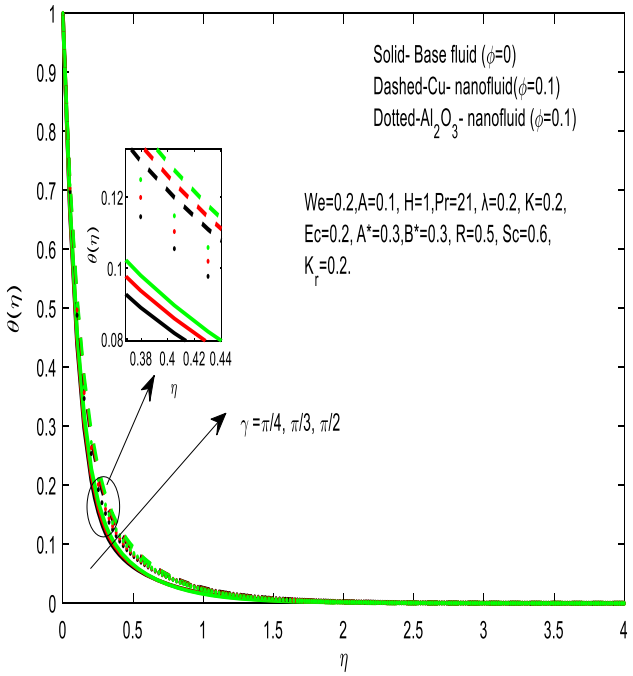

Fig. 24 Temperature profiles for γ

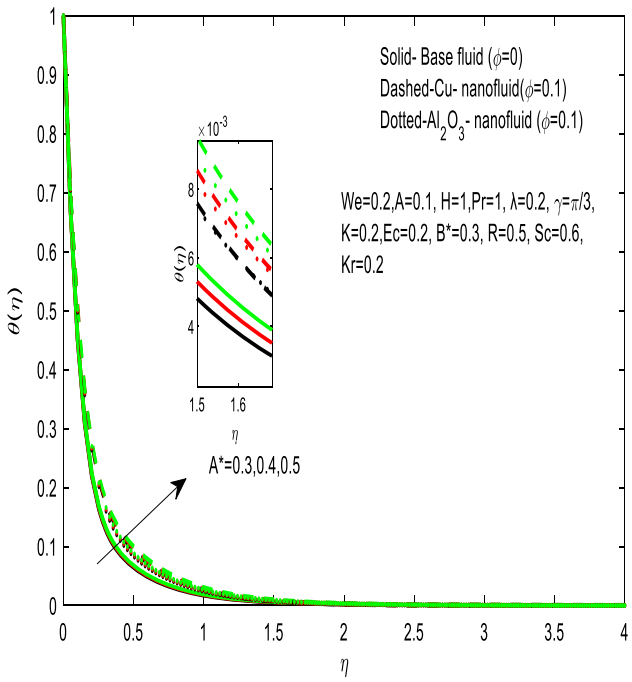

Fig. 25 Temperature profiles for A^*

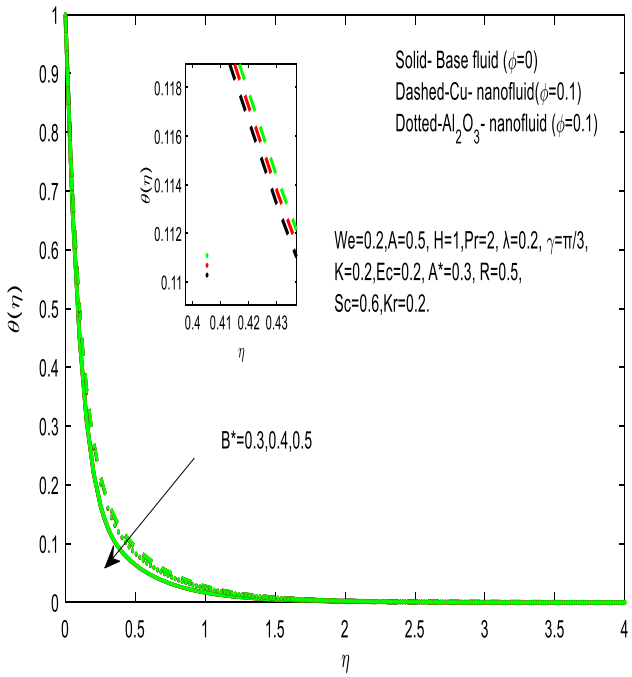

Fig. 26 Temperature profiles for B^*

fluid The effects of A^* and B^* on the temperature distribution are shown in Figs. 25 and 26. We noticed that higher values of non-uniform heat source/sink parameters boost the temperature distribution. In general the presence of heat source/sink generates the internal heat energy in the flow. Due to that we spotted an enhancement in the temperature distribution for positive values of A^* and B^*. It is observed that a nanofluid is more powerful than pure fluid

From Fig. 27, we have seen that the temperature field is a reducing function of R. Physically the radiation heat transfer dominates the convection at high temperature levels. Thus, the thermal radiation reduces the rate of heat transfer on the surface which improves the rate of cooling for thin film flow. Figure 28 describes the temperature distribution of both pure and nanofluids for various values of the Eckert number. We noticed

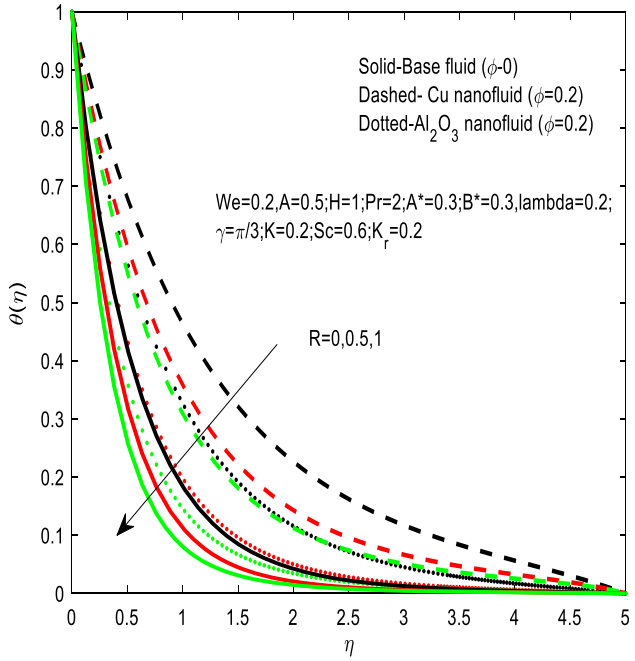

Fig. 27 Temperature profiles for R

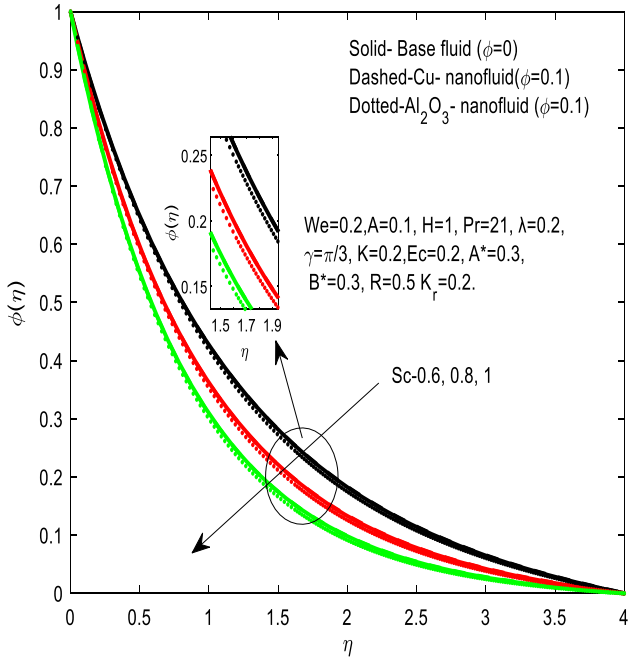

Fig. 29 Concentration for Sc

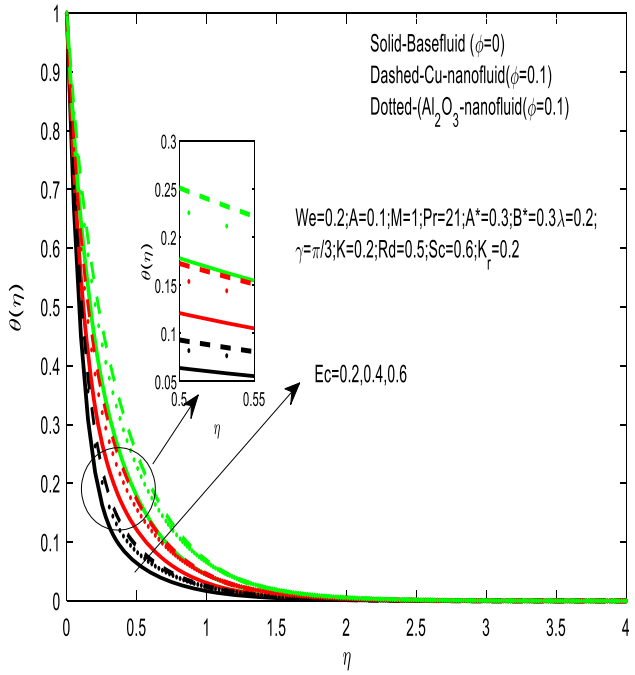

Fig. 28 Temperature profiles for Ec

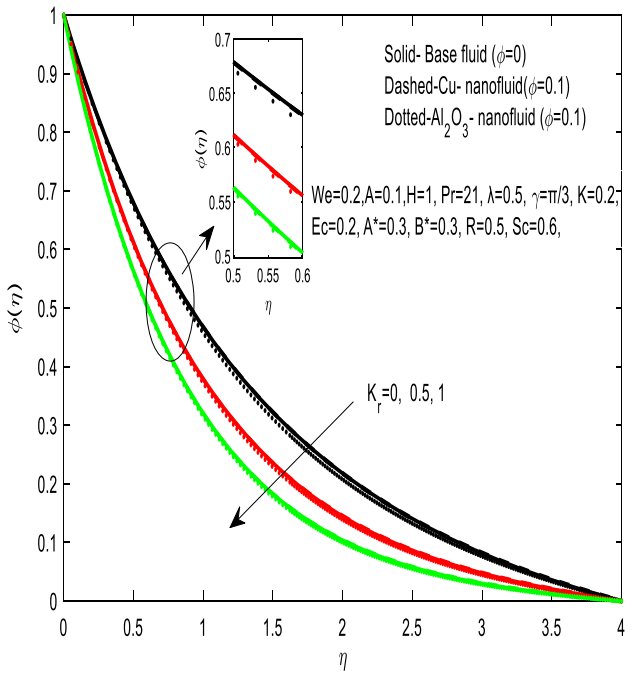

Fig. 30 Concentration fo K_{r}

the temperature boost in rising values of Eckert number. Basically, viscous dissipation improves the thermal conductivity of the fluid which leads to the improvement of the temperature field. The variation in concentration distribution for various values of Sc and K_{r} is displayed in Figs. 29 and 30. We determined that the concentration distribution is a falling function of Sc and K_{r}.

Figure 31 explores the effect of solid volume fraction (containing Copper and Al_2O_3 nanoparticles in the base fluid) on the temperature field. We observed that the rising values of solid volume fraction of the nanoparticles increasing the temperature. It is evident that for

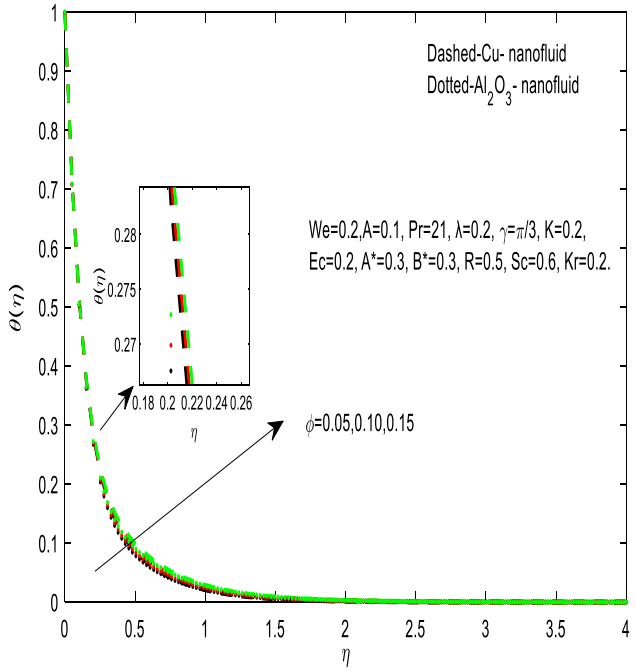

Fig. 31 Temperature profiles for ϕ

the rising values of ϕ temperature profile enhances and the accompanying thermal boundary layer thickness increases. It happens due to dispersion of nano particles.

The thermophysical properties of different nanoparticles are shown in Table 1. Table 2 describes the validation of the present results with the existing literature [41–45]. We have seen an excellent agreement between the present and past results. Tables 3 and 4 present the influence of various nondimensional parameters on the skin friction, heat and mass transfer rates of Cu and Al_2O_3 nanofluids. The coefficient of skin friction enhances for increasing values of the magnetic parameter and the reverse behaviour is identified for heat and mass transfer rates. An increase in the fluid parameter reduces the friction parameter and increases the rate of heat and mass transfer. Large values of the unsteadiness and suction/injection parameters enhance the skin friction, heat and mass transfer rates The increase in the porosity parameter enriches the friction factor and decreases the rate of heat and mass transfer. An increase in the inclined angle of the magnetic field enhances the coefficient of skin friction. It is also perceived that the growth in the non-uniform heat source/sink and Eckert number declines heat transfer rate and increases the coefficient of skin friction and the rate of mass transfer The friction factor enhances for larger values of nanoparticle volume fraction and increase the rate heat and mass transfer. The rate of mass transfer enhances for Schmidt number and chemical reaction parameter.

Table 1 Thermo-physical properties of base fluid and nanoparticles [25,28,48,49]

Physical properties	Base fluid Blood	Copper (Cu)	Silver (Ag)	Alumina (Al_2O_3)	Titanium oxide (TiO_2)	Magnesium oxide (MgO)
$\rho\,(\mathrm{kg/m^3})$	1063	8933	10500	3970	4250	3580
$C_p\,(\mathrm{J/kgK})$	3594	385	235	765	686.2	960
$k\,(\mathrm{W/mK})$	0.492	401	429	40	8.9538	48.4
$\beta \times 10^{-5}$	0.18	1.67	1.89	0.85	0.9	1.26

Table 2 Validation of the results (where We $= 0$, $H = 0$, $f_w = 0$, $\gamma = 0, K = 0$, $R = 0$, $A* = 0$, $B* = 0$, Ec $= 0$, Sc $= 0$, $K_r = 0$, $\phi = 0$)

A	λ	Pr	Grubka and Bobba [41] $-\theta'(0)$	Ali [42] $-\theta'(0)$	Ishak et.al [43] $-\theta'(0)$	Mahdy [44] $-\theta'(0)$	Navid foreidoonimehr [45] $-\theta'(0)$	Present values $-\theta'(0)$
0	0	0.72	0.8086	0.8058	0.8086	0.80868	0.80863135	0.815780
		1	1.0000	0.9961	1.0000	1.00000	1.00000000	1.001396
		3	1.9237	1.9144	1.9237	1.92368	1.92368259	1.923025
		7	3.0723	3.7006	3.0723	3.07224	3.07225021	3.071756
		10	3.7207	3.7006	3.7207	3.72067	3.72067390	3.720216
	1	1			1.0873	1.08727	1.08727817	1.086797
	2				1.1423	1.14233	1.14233930	1.141915
	3				1.1853	1.18528	1.18529032	1.184959
1	0	1	-		1.6820	1.68197	1.68199249	1.681987
	1				1.7039	1.70390	1.70391282	1.703902

Table 3 Variations in skin friction, Nu_x and Sh_x for different non-dimensional parameters

H	We	λ	A	K	f_w	γ	*Cu-nanofluid*			Al_2O_3-nanofluid		
							$-C_{fx}$	Nu_x	Sh_x	$-C_{fx}$	nu_x	sh_x
0							1.187042	10.55430	−0.912241	1.136760	10.864640	−0.927485
1							1.351661	9.932405	−0.889672	1.325068	10.170385	−0.900335
2							1.485794	9.366718	−0.871697	1.473032	9.548896	−0.879491
	0.1						1.547283	9.612262	−0.881415	1.519308	9.862033	−0.891978
	0.3						1.184302	10.240427	−0.898371	1.160296	10.462735	−0.909029
	0.5						0.920295	10.811578	−0.917044	0.902652	10.994539	−0.927335
		−0.5					1.768666	8.615451	−0.861156	1.463298	9.804915	−0.891296
		0.					1.478932	9.587585	−0.881556	1.365354	10.068984	−0.897757
		0.5					1.147668	10.403780	−0.901799	1.263426	10.318002	−0.904195
			1				1.579544	14.371640	−1.349068	1.499263	14.621273	−1.356028
			2				1.764917	17.945862	−1.709431	1.653031	18.209323	−1.715081
			3				1.908396	20.883231	−2.002588	1.778204	21.153812	−2.007452
				0.1			1.317892	10.060033	−0.893856	1.287912	10.309645	−0.905225
				0.2			1.351661	9.932405	−0.889672	1.325068	10.170385	−0.900335
				0.3			1.384436	9.805866	−0.885645	1.360933	10.032644	−0.8955658
					−0.5		0.947958	2.733964	−0.751732	1.077448	2.627665	−0.751732
						0	1.287620	7.845441	−0.863102	1.284493	7.991445	−0.863102
					0.5		1.584294	21.178047	−1.009660	1.482126	21.769239	−1.009660
						$\pi/4$	1.300799	10.132674	−0.896594	1.267774	10.392812	−0.908539
						$\pi/3$	1.351661	9.932405	−0.889672	1.325068	10.170385	−0.900335
						π /2	1.399193	9.738274	−0.883253	1.377987	9.956026	−0.892818

Table 4 Variations in skin friction, Nu_x and Sh_x for different non-dimensional parameters

A^*	B^*	Rd	Ec	Sc	Kr	ϕ	*Cu–water*			Al_2O_3–water		
							$-C_{fx}$	nu_x	sh_x	$-C_{fx}$	nu_x	sh_x
0.3							1.351661	9.932405	−0.889672	1.325068	10.170385	−0.900335
0.4							1.349876	9.864719	−0.889975	1.324603	10.116004	−0.900416
0.5							1.348084	9.932405	−0.890279	1.324137	10.06162	−0.900497
	0.3						1.351661	9.932405	−0.900335	1.325068	10.170385	−0.900335
	0.4						1.351313	9.897343	−0.900416	1.324989	10.144805	−0.900343
	0.5						1.350963	9.862141	−0.900497	1.324910	10.119149	−0.900351
		0					1.324017	4.604251	−0.891823	1.316059	4.684329	−0.901046
		0.5					1.351661	9.932405	−0.889672	1.325068	10.170385	−0.900335
		1					1.364549	16.663713	−0.888910	1.329287	17.117191	−0.900084
			0.2				1.351661	9.932405	−0.889672	1.325068	10.170385	−0.900335
			0.4				1.308192	7.463518	−0.894755	1.311626	7.696139	−0.901971
			0.6				1.266042	5.289416	−0.899772	1.298323	5.317710	−0.903600
				0.6			1.351661	9.932405	−0.889672	1.325068	10.170385	−0.900335
				0.8			1.351661	9.932405	−1.056283	1.325068	10.170385	−1.068075
				1.0			1.351661	9.932405	−1.208510	1.325068	10.170385	−1.220965
					0		1.351661	9.932405	−0.803046	1.325068	10.170385	−0.815599
					0.5		1.351661	9.932405	−1.002466	1.325068	10.170385	−1.011188
					1		1.351661	9.932405	−1.161119	1.325068	10.170385	−1.167851
						0.05	1.253034	9.919197	−0.878010	1.230567	10.162840	−0.889010
						0.10	1.351661	9.932405	−0.889672	1.325068	10.170385	−0.900335
						0.15	1.463445	9.939928	−0.901714	1.432452	10.171369	−0.911922

5 Conclusions

The present work explores the heat and mass transfer effects of MHD Williamson nanofluid over an unsteady stretching surface in the presence of radiation, viscous dissipation, non-uniform heat source/sink, chemical reaction and an inclined magnetic field. This study has application to energy industry since Cu-nanofluid has greater heat transfer rate (due to greater thermal conductivity property of copper). Further, thermal boundary layer thickness can be increased by considering the viscous dissipation effects. The present study is also useful for medical technology since copper nanoparticle suspension in viscous fluids are considered for the

treatments of various cancers and pancreatic tumours. Furthermore, alumina oxide nanoparticle suspension in viscous fluids is considered in cosmetic industries and food technology. The important findings of this study presented as follows.

(i) The inclined angle of the magnetic field braces the magnetic field and it has the potential to slow down the velocity Nusselt number and mass transfer rate whereas it increases the skin friction coefficient.
(ii) The thermal boundary layer thickness rises with an increase in Ec
(iii) Increasing values of suction/Injection parameter enhance the skin friction, Nusselt number and mass transfer rate.
(iv) The momentum boundary layer thickness of Al_2O_3 nanofluid is higher than Cu nanofluid.
(v) The thermal boundary layer thickness of Cu nanofluid is higher than Al_2O_3 nanofluid

Author contribution statement

The authors R.M. and P.L. provided the idea, formulation of the problem, methodology and worked on the details of the problem. The author K.V. worked on the details of the problem, several drafts of the manuscript and presented the final version of the manuscript. All authors approve the final version for publication.

References

1. S.U.S. Choi, Enhancing thermal conductivity of fluids with nanoparticles, developments and applications of non-Newtonian flows. Am. Soc. Mech. Eng. **66**, 99–105 (1995)
2. J.A. Eastman, U.S. Choi, S. Li, S.J. Thompson, S. Lee, Enhanced thermal conductivity through the development of nanofluids. Mater. Res. Soc. Sympos. Proce. **457**, 3–11 (1997)
3. X. Hang, I. Pop, X.-C. You, Flow and heat transfer in a nanoliquid film over an unsteady stretching surface. Int. J. Heat Mass Transf. **60**, 646–652 (2013)
4. K. Vajravelu, K.V. Prasad, Chiu-On Ng, Unsteady convective boundary layer flow of a viscous fluid at a vertical surface with variable fluid properties. Nonlinear Anal. Real World Appl. **14**(1), 455–464 (2013)
5. Y. Lin, L. Zheng, G. Chen, Unsteady flow and heat transfer of pseudo-plastic nanoliquid in a finite thin film on a stretching surface with variable thermal conductivity and viscous dissipation. Powder Technol. **274**, 324–332 (2015)
6. N. Sandeep, B. Rushi Kumar, M.S. Jagadeesh Kumar, A comparative study of convective heat and mass transfer in non-Newtonian nanofluid flow past a permeable stretching sheet. J. Mol. Liq. **212**, 585–591 (2015)
7. P. Sudarsana Reddy, A.J. Chamkha, A. Al-Mudhaf, MHD heat and mass transfer flow of nanofluid over an inclined vertical porous plate with radiation and heat generation/absorption. Adv. Powder Technol. **28**, 1008–1017 (2017)
8. S. Nadeem, R.U. Haq, Z.H. Khan, Numerical study of MHD boundary layer flow of a Maxwell fluid past a stretching sheet in the presence of nanoparticle. J. Taiwan Inst. Chem. Eng. **45**, 121–126 (2014)
9. M. Sheikholeslami, D.D. Ganji, M.M. Rashidhi, Magnetic field effect on unsteady nanofluid flow and heat transfer using Buongiorno model. J. Magnet. Magnet. Mater. **416**, 164–173 (2016)
10. P.K. Kameswaran, M. Narayana, P. Sibanda, P.V.S.N. Murthy, Hydromagnetic nanofluid flow due to a stretching or shrinking sheet with viscous dissipation and chemical reaction effects. Int. J. Heat Mass Transf. **55**, 7587–7595 (2012)
11. S. Nadeem, S.T. Hussain, C. Lee, Flow of Williamson fluid over a stretching sheet. Braz. J. Chem. Eng. **30**(3), 619–625 (2013)
12. S. Nadeem, S.T. Hussain, Flow and heat transfer analysis of Williamson nanofluid. Appl. Nanosci. **4**, 1005–1012 (2014)
13. S. Nadeem, S.T. Hussain, Heat transfer analysis of Williamson fluid over exponentially stretching surface. Appl. Math. Mech. **35**(4), 489–502 (2014)
14. M. Ramzan, M. Bilal, J.D. Chung, Radiative Williamson nanofluid over a convectively heated Riga plate with chemical reaction-A numerical approach. Chin. J. Phys. **55**(4), 1663–1673 (2017)
15. T. Hayat, A. Shafiq, A. Alsaedi, Hydromagnetic boundary layer flow of Williamson fluid in the presence of thermal radiation and ohmic dissipation. Alex. Eng. J. **55**, 2229–2240 (2016)
16. Z. Shah, E. Bonyah, S. Islam, W. Khan, M. Ishaq, Radiative MHD thin film flow of Williamson fluid over an unsteady permeable stretching sheet. Heliyon. **4**(10), e00825 (2018)
17. A. Zaib, R.U. Haq, A.J. Chamkha, M.M. Rashidhi, Impact of non-linear radiative nanoparticle on the unsteady flow of Williamson fluid toward a permeable convectively heated shrinking sheet. World J. Eng. **15**(6), 731–742 (2018)
18. M. Khan, A. Khan, Influence of non-linear thermal radiation on the 2D unsteady flow of a Williamson fluid with heat source/sink. Results Phys. **7**, 3968–3975 (2017)
19. A. Hamid, M. Khan, A.S. Alshomrani, Non-linear radiation and chemical reaction effects on slip flow of Williamson nanofluid due to static/moving wedge. Appl. Nanosci. (2019)
20. J. Raza, F. Mebarek-Oudina, B. Mahanthesh, Magnetohydrodynamic flow of nano Williamson fluid generated by stretching plate with multiple slips. Multidiscip. Model. Mater. Struct. **15**(5), 871–894 (2019)
21. T. Hayat, S. Nawaz, A. Alsaedi, M. Rafiq, Influence of radial magnetic field on the peristaltic flow of Williamson fluid in a curved complaint walls channel. Results Phys. **7**, 982–990 (2017)
22. M. Sheikholeslami, D.D. Ganji, M. Younus Javed, R. Ellahi, Effect of thermal radiation on magnetohydrodynamics nanofluid flow and heat transfer by means of two-phase model. J. Magnet. Magnet. Mater. **374**, 36–43 (2015)
23. A. Ishak, N. Azizah Yacob, N. Bachok, Radiation effects on the thermal boundary layer flow over a moving plate

with convective boundary condition. Meccanica. **46**, 795–811 (2011)
24. B. Mahanthesh, B.J. Gireesha, R. Subba, R. Gorla, Heat and mass transfer effects on the mixed convective flow of chemically reacting nanofluid past a moving/stationary vertical plate. Alex. Eng. J. **55**(1), 569–581 (2016)
25. N.S. Elgazery, Nanofluids over a permeable unsteady stretching surface with non-uniform heat source/sink in the presence of the inclined magnetic field. J. Egypt. Math. Soc. **27**(1), 9 (2019)
26. T. Hayat, S. Qayyum, M. Imtiaz, A. Alsaedi, Comparative study of silver and copper water nanofluids with mixed convection and nonlinear thermal radiation. Int. J. Heat Mass Transf. **102**, 723–732 (2016)
27. K. Vajravelu, K.V. Prasad, J. Lee, I. Changhoon Lee, R.A. Pop, V. Gorder, Convective heat transfer in the flow of viscous Ag-water and Cu-water nanofluids over a stretching surface. Int. J. Thermal Sci. **50**, 843–851 (2011)
28. A.M. Rohini, S. Ahmad, I. Pop, Flow and heat transfer over an unsteady shrinking sheet with suction in nanofluids, Int. J. Heat Mass Transf. **55**, 1888–1895 (2012)
29. C. Sulochana, G.P. Ashwin Kumar, Carreau model for liquid thin film flow of dissipative magnetic-nanofluids over a stretching sheet. Int. J. Hybrid Inf. Technol. **10**(1), 239–254 (2017)
30. Ch. Achi Reddy, B. Shankar, Unsteady convective boundary layer flow of nanofluid over a stretching sheet in the presence of viscous dissipation, chemical reaction and porous medium. Mater. Today Proc. **4**, 7484–7497 (2017)
31. T. Motsumi, O.D. Makinde, Effects of thermal radiation and viscous dissipation on boundary layer flow of nanofluids over a permeable moving flat plate. Phys. Scr. **86**(4), 045003 (2012)
32. G. Sucharitha, K. Vajravelu, P. Lakshminarayana, Effect of heat and mass transfer on the peristaltic flow of a Jeffrey nanofluid in a tapered flexible channel in the presence of the aligned magnetic field. Eur. Phys. J. Spec. Top. **228**, 2713–2728 (2019)
33. C.S.K. Raju, N. Sandeep, C. Sulochana, V. Sugunamma, M. Jayachandra Babu, Radiation, inclined magnetic field, cross diffusion effects on flow over a stretching surface. J. Nigerian Math. Soc. **34**, 169–180 (2015)
34. M. Krishna Murthy, S. Sreenadh, P. Lakshminarayana, G. Sucharitha, B. Rushikumar, Thermophoresis and Brownian motion effects on three dimensional MHD slip flow of a Casson nanofluid over an exponentially stretching surface. J. Nano Fluids **8**(6), 1267–1272 (2019)
35. G. Sucharitha, M.M. Rashidi, S. Sreenadh, P. Lakshminarayana, Effects of magnetic field and slip on convective peristaltic flow of a non-Newtonian fluid in an inclined non-uniform porous channel with flexible walls. J. Porous Media **21**(10), 895–910 (2018)
36. G. Kumaran, P. Lakshminarayana, P.B.A. Reddy, N. Sandeep, Melting Heat Transfer in Magnetohydrodynamic Carreau Fluid over a Thermally Stratified Parabolic Surface. Defect Diffus. Forum **388**, 246–264 (2018)
37. G. Sucharitha, K. Vajravelu, P. Lakshminarayana, Magnetohydrodynamic nanofluid flow in a non-uniform aligned channel with joule heating. J. Nanofluids **8**(7), 1373–1384 (2019)
38. R. Meenakumari, P. Lakshminarayana, K. Vajravelu, Influence of induced magnetic field and slip conditions on convective Prandtl fluid flow over a stretching surface with homogeneous and heterogeneous reactions. Multidiscip. Model. Mater. Struct. (2020). https://doi.org/10.1108/MMMS-02-2020-0040
39. R. Meenakumari, P. Lakshminarayana, Radiation and Hall effects on a 3D flow of MHD Williamson fluid over a stretchable surface. Heat Transf. (2020). https://doi.org/10.1002/htj.21833
40. P. Lakshminarayana, K. Vajravelu, G. Sucharitha, S. Sreenadh, Peristaltic slip flow of a Bingham fluid in an inclined porous conduit with Joule heating. Appl. Math. Nonlinear Sci. **3**(1), 41–54 (2018)
41. L.J. Grubka, K.M. Bobba, Heat transfer characteristics of a continuous stretching surface with variable temperature. J. Heat Transf. **107**, 248–250 (1985)
42. M.E. Ali, Heat transfer characteristics of a continuous stretching surface. Heat Mass Transf. **29**, 227–234 (1994)
43. A. Ishak, R. Nazar, I. Pop, Boundary layer flow and heat transfer over an unsteady stretching vertical surface. Meccanica. **44**, 369–375 (2009)
44. A. Mahdy, Unsteady mixed convection boundary layer flow and heat transfer of nanofluids due to stretching sheet. Nucl. Eng. Des. **249**, 248–255 (2012)
45. N. Freidoonimehr, M. Mehdi, M. Rashidi, S. Mahmud, Unsteady MHD free convective flow past a permeable stretching vertical surface in a nanofluid. Int. J. Thermal Sci. **87**, 136–145 (2015)
46. M. Vinodkumar Reddy, P. Lakshminarayana, MHD radiative flow of a Maxwell fluid on an expanding surface with the effects of Dufour and Soret and chemical reaction. Comput. Thermal Sci. **12**(4), 317–327 (2020)
47. K. Subbarayudu, S. Suneetha, P. Bala Anki Reddy, The assessment of time dependent flow of Williamson fluid with radiative blood flow against a wedge. Propuls. Power Res. **9**(1), 87–99 (2020)
48. N.S. Elgazery, Flow of non-Newtonian magneto-fluid with gold and alumina nanoparticles through a non-Darcian porous medium. J. Egypt. Math. Soc. **27**(39), 27–39 (2019)
49. A. Zaman, N. Ali, N. Kousar, Nano particles (Cu, TiO_2, Al_2O_3) analysis on unsteady blood flow through an artery with a combination of stenosis and aneurysm. Comput. Math. Appl. **76**(9), 2179–2191 (2018)